Photoelectron Holography of a Heteronuclear Molecule

Marko Haertelt,[1,*,†] WenZhuo Wu,[2,*] XuanYang Lai,[2,‡] Andrei Yu. Naumov,[1] XiaoJun Liu,[2] Paul B. Corkum,[1] and André Staudte[1,§]

[1]*Joint Laboratory for Attosecond Science of the National Research Council and the University of Ottawa, Ottawa, 100 Sussex Drive, Ontario K1A 0R6, Canada*

[2]*State Key Laboratory of Magnetic Resonance and Atomic and Molecular Physics, Wuhan Institute of Physics and Mathematics, Innovation Academy for Precision Measurement Science and Technology, Chinese Academy of Sciences, Wuhan 430071, China*

(Received 13 March 2025; revised 7 January 2026; accepted 20 February 2026; published 15 April 2026)

We present strong-field photoelectron holography measurements of hydrogen chloride (HCl) that resolve subcycle dynamics in two ionization channels associated with the HOMO and HOMO-1 orbitals. The holograms in the photoelectron momentum distributions show different cutoffs and interference fringes tied to orbital-specific ionization potentials. Furthermore, molecular-frame photoelectron holograms from oriented HCl exhibit pronounced asymmetries that arise from the interplay of the molecular dipole and the ionic Coulomb field. These findings establish strong-field photoelectron holography as a sensitive probe of subcycle electron wave packet dynamics in polar molecules.

DOI: 10.1103/z4xn-m554

Strong-field photoelectron holography [1,2] allows nuclear and electron dynamics to be studied on a sub-laser-cycle timescale [3–7]. In direct analogy to the original idea of electron holography [8], a strong-field hologram is created by the interference of the scattered (signal) and the unscattered (reference) part of an electron wave packet. In contrast to conventional holography, the electron wave packet is produced via optical tunnel ionization directly from the scattering object. Consequently, the ionizing orbital shapes the photoelectron scattering wave packet in amplitude and phase [9–11], leaving a fingerprint in the strong-field photoelectron hologram [6,12,13].

Polar molecules provide an opportunity to directly compare the strong-field holograms for the different sides of the molecule. The final hologram not only will reflect the anisotropy of the electron density at the instant of ionization, but it will also encode the charge distribution in the molecular ion during the initial departure and subsequent rescattering of the electron wave packet [14,15]. However, strong-field photoelectron holography of oriented heteronuclear molecules has been, so far, limited to theoretical studies [14–16].

Here, we present experimentally obtained photoelectron holograms of a heteronuclear molecule. Specifically, we study the photoelectron holograms correlated to the two different ionization channels of HCl. First, ignoring orientation, we observe differences in the holograms for ionization from the highest occupied molecular orbital (HOMO) and the HOMO-1, which are readily populated and separable in optical tunnel ionization, as shown in [17]. To the best of our knowledge, this represents the first instance of simultaneous photoelectron holography from different orbitals, and our modeling of the process suggests that the different saturation intensities for the two channels are responsible for the subtle difference in the photoelectron spectra. For the HOMO-1 channel, we can also obtain photoelectron holograms of oriented molecules. We observe asymmetric holograms that encode information about the side from which the molecule is ionized.

HCl is a simple polar molecule with a moderate permanent dipole moment of 1.1D. Experimentally, polar molecules can be actively oriented in space with optical laser pulses [18–22], but the degree of orientation is often low. However, in intense laser fields, HCl lends itself to *a posteriori* determination of the molecular orientation [17].

The concept of the experiment is illustrated in Fig. 1(a). Under an intense infrared laser field, HCl is tunnel-ionized into either its ground state $X^2\Pi$ (corresponding to ionization of HOMO) or its first excited state $A^2\Sigma^+$ (corresponding to ionization of HOMO-1) of HCl^+ [17]. In the presence of the laser field, the A state strongly couples to the dissociative ($2^2\Sigma^+$) state, enabling bond softening [23] and resulting in fragmentation into $H + Cl^+$ or $H^+ + Cl$. By contrast, the X state, which is accessed via a transition perpendicular to the molecular axis, lacks a direct pathway to dissociation. To

*These authors contributed equally to this work.
†Contact author: marko.haertelt@iaf.fraunhofer.de
‡Contact author: xylai@wipm.ac.cn
§Contact author: andre.staudte@nrc.ca

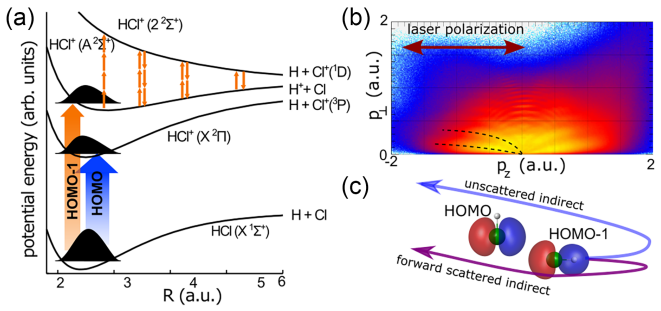

FIG. 1. (a) Schematic diagram for ionization and subsequent dissociation pathways of HCl in an intense near-infrared laser field (a.u., atomic units). (b) Example of a measured, uncorrelated PMD using the cylindrical symmetry imposed by the laser polarization (along z). The PMD exhibits holographic interference structures (dashed lines). Small left-right differences arise from instrumental asymmetries of the spectrometer and are not related to molecular orientation. (c) Tunnel ionization along the highest orbital density gives rise to different effective alignments for HOMO and HOMO-1. The interference of unscattered and scattered indirect (recollision) trajectories causes the holographic structures.

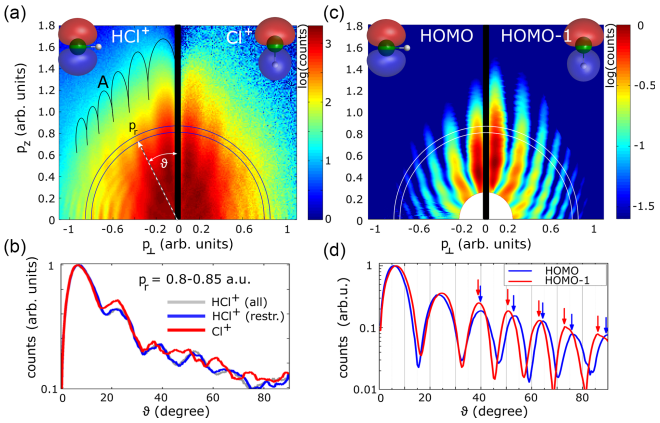

FIG. 2. (a) Measured normalized PMDs (on a log10 scale) correlated with the single (nondissociative) ionization of HCl and the dissociative ionization (Cl^+ fragment). For both distributions, we make use of the C_s symmetry and show only the electrons ejected toward the electron detector. The strong-field holographic interference due to forward scattering is indicated as feature A. (b) Radially integrated momentum distributions within the indicated semicircles in (a). For HCl^+, we also show the curve for a reduced number of events in blue. The curves with low statistics are smoothed with a five-point moving average. (c) Simulated PMDs for HOMO (left) and HOMO-1 (right). See text for details. (d) Same as (b) for the simulated PMDs.

determine the molecular orientation, we analyze the ion momentum from the dissociative $A-(2^2\Sigma^+)$ channel, where the fragment momentum remains aligned with the initial molecular axis.

In Fig. 1(b), we show a representative photoelectron momentum distribution (PMD) plotted in the electron momentum components parallel and perpendicular to the linear laser polarization (here and throughout the Letter, a.u. denotes atomic units). The PMD displays a clear strong-field photoelectron hologram, which is formed by the interference of unscattered indirect and forward-scattered indirect recollision electron trajectories. Depending on the time of ionization within the laser cycle, two different electron trajectories are distinguished in linearly polarized light: direct and indirect electrons. Whereas direct electrons do not return to the ion, scattered and unscattered indirect electrons are responsible for the holographic interference, as illustrated in Fig. 1(c). In addition, based on the spatial distribution of the orbital electron densities shown in Fig. 1(c), ionization from the HOMO predominantly selects molecules aligned perpendicular to the laser polarization, whereas ionization from HOMO-1 and subsequent dissociation favor molecules aligned parallel to it [17].

The correlated three-dimensional electron and ion momentum distributions were measured using a COLTRIMS apparatus [24]. For ionization linearly polarized, 28 fs pulses centered at a wavelength of 800 nm were focused to an intensity of $(2.1 \pm 0.2) \times 10^{14}$ W/cm^2 into a gas mixture of 10% HCl in helium. For further details see the Supplemental Material [25].

To aid the interpretation of the experimentally observed features, we simulate the PMDs using the Coulomb quantum-orbit strong-field approximation (CQSFA) [26–30] extended to heteronuclear molecular systems to describe photoelectron holography originating from different ionization channels; for details, see Ref. [25].

Previous predictions of strong-field photoelectron holography in atoms indicated that the ionizing orbital affects the shape and angular extent of the holographic fringes [3]. Here, we analyze our measurements in this context and find that several of these qualitative trends are reproduced experimentally.

In Fig. 2(a), we show the normalized PMDs correlated with HCl^+ and Cl^+. We make use of the cylindrical symmetry of the momentum distribution but restrict our analysis to electrons that go toward the electron detector. Both channels exhibit holographic fringes (structure A, black line) and above-threshold ionization (ATI) rings separated by the photon energy (blue semicircles). Small but distinct differences are apparent. Importantly, these differences are not a consequence of the nearly 2-orders-of-magnitude difference in event yield between the two channels, as they persist when the same number of events is selected for both channels (see Ref. [25]).

In Fig. 2(b), we isolate forward scattering interference from ATI by integrating over a specific radial momentum range (indicated by the two semicircles; for other ranges, see Ref. [25]). Since ATI depends only weakly on the emission direction, this isolates the holographic signal. For consistency, the HCl^+ data were also downsampled to match the statistics of the Cl^+ channel.

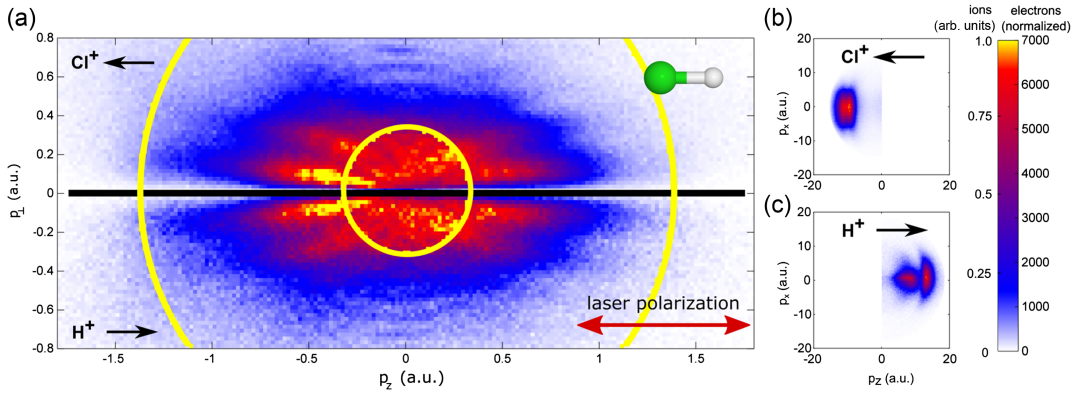

FIG. 3. (a) Normalized photoelectron hologram for oriented HCl in a linearly polarized laser field during single-ionization-induced dissociation. Positive perpendicular electron momenta $p_\perp$ correspond to the Cl^+ fragment (coincident with a neutral H), while negative $p_\perp$ correspond to the H^+ fragment. The hologram shows higher intensity and a more clearly resolved "spider" structure in the chlorine direction. (b),(c) Correlated ion momentum distribution.

While the HCl^+ signal is more pronounced, both channels exhibit multiple interference maxima. In the Cl^+ channel, these maxima are shifted toward smaller emission angles. Furthermore, the holographic interferences along the laser polarization direction differ between the two channels. For example, the cutoffs, i.e., the maximum momenta, of the first two fringes are higher for ionization from HOMO-1, and the intensity ratio between the first two peaks is reduced, as seen in Fig. 2(b). These observations demonstrate that the two ionization channels produce distinct and reproducible holographic patterns.

Figure 2(c) shows simulated PMDs for ionization from the HOMO (left) and HOMO-1 (right), calculated using the Coulomb quantum-orbit strong-field approximation extended to molecular systems [26–30]. Our model incorporates the molecular structure of HCl and the corresponding initial-state wave functions (see Ref. [25] for details).

The simulations reproduce the main experimental trends, including the larger cutoff momentum for HOMO-1 and the contraction of the interference fringes toward smaller emission angles, as shown in Fig. 2(d). Remaining discrepancies in fringe position and contrast arise from model approximations and experimental factors such as intensity fluctuations and finite detector resolution.

Our model allows us to interpret the observations above. The different ionization potentials of 12.747 and 16.265 eV for HOMO and HOMO-1, respectively, cause the two channels to experience different effective intensities within the laser pulse. A higher intensity is directly responsible for a larger cutoff momentum [31]. It also causes longer trajectories and thereby a larger phase accumulation, which leads to the narrowing of the holographic interferences (see Ref. [25]).

This analysis establishes that HCl allows a clean experimental separation of holograms associated with the HOMO and HOMO-1 channels. Importantly, this channel separation does not rely on the heteronuclear nature of the molecule. The heteronuclear aspect enters only through the orientation dependence discussed in the following section.

Next, we concentrate on orientation dependence. Only the HOMO-1 channel offers access to the molecular orientation in our setup. Because the bond-softening process requires an electric field pointing along the molecular axis, neither Cl^+ nor H^+ ions are observed perpendicular to the light polarization (along z). This allows us to distinguish two molecular orientations with respect to our laboratory frame, i.e., the chlorine atom pointing toward or away from the ion detector. Photoelectron momentum distributions for these two molecular orientations can be measured in the Cl^+ or H^+ channel. As shown in [25], the observed orientation-dependent asymmetry persists for all laboratory-frame emission directions and is not restricted to a particular projection.

In Fig. 3(a), we show the results for the two dissociation channels yielding either a Cl^+ or H^+ in the upper and the lower half of the figure, respectively. In subfigures (b) and (c), we show the corresponding ion momenta. Because the fragment momentum remains aligned with the initial molecular axis, we determine orientation cosines $\langle \cos\theta \rangle$ between 0.90 and 0.93. The near identity of the upper and lower halves of the PMD shows that the ionization and subsequent scattering are largely independent of the specific dissociation channel or the laboratory-frame orientation of the molecule [25].

The outer yellow circle in Fig. 3(a) is the $2\sqrt{U_p}$ momentum cutoff for the direct electron trajectory, with U_p being the ponderomotive potential. The forward scattering interference structure extends to larger momenta toward the chlorine side than the hydrogen side. Classical trajectory simulations have shown that the Coulomb field of the parent ion reduces the cutoff momenta for direct electrons, as they experience a negative acceleration, whereas indirect electrons experience a positive acceleration by the ionic potential, and their cutoff energy increases [44]. Hence,

the asymmetry in the PMD indicates an asymmetry of ionization between the two sides of the molecule, albeit asymmetric holography patterns may also be observed in homonuclear molecules if the symmetry of the driving field lacks inversion symmetry [30].

The inner yellow circle in Fig. 3(a) at $p_r = \sqrt{p_\perp^2 + p_z^2} = 0.3$ a.u. corresponds to the maximum photoelectron momentum for an electron returning twice to the parent ion. The structures within that circle have been attributed to higher order holographic interferences based on multiple returns [4]. We can clearly see a qualitative difference in this region depending on the molecular orientation relative to the photoelectron.

In both channels, we observe asymmetric forward scattering interference structures that have a higher contrast toward the chlorine side of the molecule. Not only does the interference structure have a larger contrast on the chlorine side, there are also more electrons ending up on the chlorine side. A quantitative analysis of this left-right asymmetry is presented in [25].

At first sight, a larger probability of finding the electron on the chlorine side seems to contradict previously published results of the angular ionization probability [17]. In fact, using circular polarization, we measured a differential ionization probability on the hydrogen side at our field strength that is 1.72 higher than on the chlorine side; see Ref. [25]. Therefore, the inversion of the ionization asymmetry must be due to the linear polarization of the laser field. In the following, we explain these observations.

We now analyze the observed ionization asymmetry in terms of the contributing photoelectron trajectories. Figure 4(a) illustrates how an ionization anisotropy and the Coulomb potential interact to create asymmetry in linearly polarized light. The ionization anisotropy in polar molecules breaks the symmetry of the ionization step. However, the laser field symmetrizes the electron current from either side of the molecule. The observable electron distribution becomes asymmetric only through the additional action of the Coulomb potential, which breaks the symmetry of direct and indirect trajectories [44,45]. Particularly, the attractive Coulomb field increases the probability of recollision. Thus, although more ionization occurs on the hydrogen side [17], the larger part of this wave packet is recolliding, ending up on the chlorine side of the molecule.

In Figs. 4(b)–4(e), we use our models to simulate the cases shown in (a) in order to confirm our interpretation. In Fig. 4(b), we have simulated ionization from a symmetric wave function using strong-field approximation (SFA) and thereby ignore the parent ion's Coulomb field. Consequently, the holographic interference fringes are absent, and intracycle interferences dominate.

Figure 4(c) shows the CQSFA simulated photoelectron momentum spectrum for a hydrogen-like symmetric wave function. The ionic Coulomb field is included in this model,

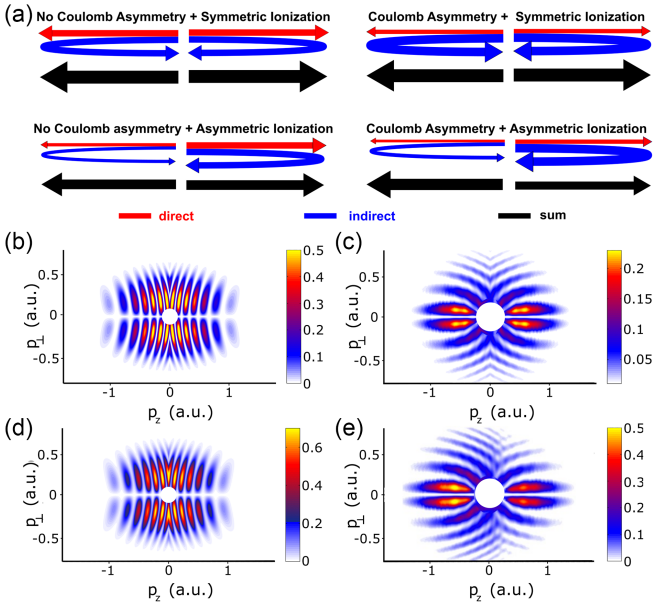

FIG. 4. (a) Schematic showing the effect of the Coulomb field and an asymmetric ionization rate on the ratio between direct and indirect electrons and their sum. (b)–(e) Simulated PMDs for ionization with corresponding parameters as in (a). See text for details.

leading to the appearance of the dominant strong-field photoelectron holographic interferences. As expected, the photoelectron momentum spectrum remains symmetric.

In Fig. 4(d), we simulate the PMD for ionization from HOMO-1 of HCl with SFA theory, for which the ionic Coulomb potential is not considered. In this case, the photoelectron momentum spectrum is still symmetric. The reason is that, due to the neglect of the Coulomb field, the ionization amplitudes of the direct and forward scattering trajectories from the same side of the molecule are the same. Thus, the two photoelectrons with the opposite momentum have the same amplitudes for the monochromatic laser field even though the initial wave function of HOMO-1 is asymmetric.

Finally, in Fig. 4(e), we show the CQSFA simulation including the Coulomb field and the asymmetric HOMO-1 of HCl with the same orientation as in the experiment in Fig. 3(a). Now, a clear left-right asymmetry can be observed. Therefore, our simulations further support the interpretation that the asymmetric interference structure in the photoelectron momentum spectrum of HCl from HOMO-1 originates from the *joint* action of the asymmetric initial wave function and the ionic Coulomb potential.

In summary, our observation of clear orientation-dependent asymmetries in the photoelectron angular distributions of HCl demonstrates that strong-field photoelectron holography is inherently sensitive to the molecular dipole and ionic Coulomb potential, even for a simple polar molecule with a moderate dipole moment. This result provides a crucial step toward extending holographic

imaging techniques to more complex, less symmetric molecules. In such systems, site-specific ionization pathways and the resulting charge migration can play a key role in ultrafast processes. The orientation sensitivity shown here provides a prerequisite for using strong-field holography to probe where ionization occurs and to track localized electron dynamics in real time in future studies. This opens promising opportunities for site-selective ionization studies and for resolving charge migration in larger heteronuclear or polyatomic molecules, offering new insights into ultrafast chemical dynamics with combined spatial and temporal resolution.

Acknowledgments—We are indebted to Michael Spanner and Michael Schuurman for helpful discussions. We thank Bert Avery and Dave Crane for technical support. We gratefully acknowledge support from CFI, CRC, Joint Centre for Extreme Photonics, the National Natural Science Foundation of China (Grants No. 12274420, No. 12450403, and No. 12121004), and the CAS Project for Young Scientists in Basic Research (Grant No. YSBR-055). M. H. thanks the Alexander von Humboldt Foundation for a Feodor-Lynen fellowship.

Data availability—The data that support the findings of this article are not publicly available upon publication because it is not technically feasible and/or the cost of preparing, depositing, and hosting the data would be prohibitive within the terms of this research project. The data are available from the authors upon reasonable request.

[1] M. Spanner, O. Smirnova, P. B. Corkum, and M. Y. Ivanov, Reading diffraction images in strong field ionization of diatomic molecules, J. Phys. B **37**, L243 (2004).
[2] Y. Huismans *et al.*, Time-resolved holography with photoelectrons, Science **331**, 61 (2011).
[3] X.-B. Bian, Y. Huismans, O. Smirnova, K.-J. Yuan, M. J. J. Vrakking, and A. D. Bandrauk, Subcycle interference dynamics of time-resolved photoelectron holography with midinfrared laser pulses, Phys. Rev. A **84**, 043420 (2011).
[4] D. D. Hickstein, P. Ranitovic, S. Witte, X.-M. Tong, Y. Huismans, P. Arpin, X. Zhou, K. E. Keister, C. W. Hogle, B. Zhang, C. Ding, P. Johnsson, N. Toshima, M. J. J. Vrakking, M. M. Murnane, and H. C. Kapteyn, Direct visualization of laser-driven electron multiple scattering and tunneling distance in strong-field ionization, Phys. Rev. Lett. **109**, 073004 (2012).
[5] M. Haertelt, X.-B. Bian, M. Spanner, A. Staudte, and P. B. Corkum, Probing molecular dynamics by laser-induced backscattering holography, Phys. Rev. Lett. **116**, 133001 (2016).
[6] S. G. Walt, N. Bhargava Ram, M. Atala, N. I. Shvetsov-Shilovski, A. von Conta, D. Baykusheva, M. Lein, and H. J. Wörner, Dynamics of valence-shell electrons and nuclei probed by strong-field holography and rescattering, Nat. Commun. **8**, 15651 (2017).
[7] G. Porat, G. Alon, S. Rozen, O. Pedatzur, M. Krüger, D. Azoury, A. Natan, G. Orenstein, B. D. Bruner, M. J. J. Vrakking, and N. Dudovich, Attosecond time-resolved photoelectron holography, Nat. Commun. **9**, 2805 (2018).
[8] D. Gabor, A new microscopic principle, Nature (London) **161**, 777 (1948).
[9] M. Meckel, D. Comtois, D. Zeidler, A. Staudte, D. Pavičić, H. C. Bandulet, H. Pépin, J. C. Kieffer, R. Dörner, D. M. Villeneuve, and P. B. Corkum, Laser-induced electron tunneling and diffraction, Science **320**, 1478 (2008).
[10] D. Comtois, H.-C. Bandulet, M. Spanner, D. Pavičić, M. Meckel, D. Zeidler, H. Pépin, R. Dörner, J.-C. Kieffer, D. Villeneuve, P. Corkum, and A. Staudte, Laser-induced orbital projection and diffraction of O_2 with velocity map imaging, J. Mod. Opt. **60**, 1395 (2013).
[11] Y. Huismans, A. Rouzée, A. Gijsbertsen, P. S. W. M. Logman, F. Lépine, C. Cauchy, S. Zamith, A. S. Stodolna, J. H. Jungmann, J. M. Bakker, G. Berden, B. Redlich, A. F. G. van der Meer, K. J. Schafer, and M. J. J. Vrakking, Photoelectron angular distributions from the ionization of xenon Rydberg states by midinfrared radiation, Phys. Rev. A **87**, 033413 (2013).
[12] M. Meckel, A. Staudte, S. Patchkovskii, D. M. Villeneuve, P. B. Corkum, R. Dörner, and M. Spanner, Signatures of the continuum electron phase in molecular strong-field photoelectron holography, Nat. Phys. **10**, 594 (2014).
[13] M. Li, X. Sun, X. Xie, Y. Shao, Y. Deng, C. Wu, Q. Gong, and Y. Liu, Revealing backward rescattering photoelectron interference of molecules in strong infrared laser fields, Sci. Rep. **5**, 8519 (2015).
[14] X.-B. Bian and A. D. Bandrauk, Orientation-dependent forward-backward photoelectron holography from asymmetric molecules, Phys. Rev. A **89**, 033423 (2014).
[15] S. Wang, J. Y. Che, C. Chen, G. G. Xin, and Y. J. Chen, Tracing the origins of an asymmetric momentum distribution for polar molecules in strong linearly polarized laser fields, Phys. Rev. A **102**, 053103 (2020).
[16] D. Habibović, A. Gazibegović-Busuladžić, M. Busuladžić, and D. B. Milošević, Strong-field ionization of heteronuclear diatomic molecules using an orthogonally polarized two-color laser field, Phys. Rev. A **103**, 053101 (2021).
[17] H. Akagi, T. Otobe, A. Staudte, A. Shiner, F. Turner, R. Dörner, D. M. Villeneuve, and P. B. Corkum, Laser tunnel ionization from multiple orbitals in HCl, Science **325**, 1364 (2009).
[18] B. Friedrich and D. Herschbach, Enhanced orientation of polar molecules by combined electrostatic and nonresonant induced dipole forces, J. Chem. Phys. **111**, 6157 (1999).
[19] M. Härtelt and B. Friedrich, Directional states of symmetric-top molecules produced by combined static and radiative electric fields, J. Chem. Phys. **128**, 224313 (2008).
[20] L. Holmegaard, J. H. Nielsen, I. Nevo, H. Stapelfeldt, F. Filsinger, J. Küpper, and G. Meijer, Laser-induced alignment and orientation of quantum-state-selected large molecules, Phys. Rev. Lett. **102**, 023001 (2009).
[21] O. Ghafur, A. Rouzée, A. Gijsbertsen, W. K. Siu, S. Stolte, and M. J. J. Vrakking, Impulsive orientation and alignment of quantum-state-selected NO molecules, Nat. Phys. **5**, 289 (2009).

[22] S. De, I. Znakovskaya, D. Ray, F. Anis, N. G. Johnson, I. A. Bocharova, M. Magrakvelidze, B. D. Esry, C. L. Cocke, I. V. Litvinyuk, and M. F. Kling, Field-free orientation of CO molecules by femtosecond two-color laser fields, Phys. Rev. Lett. **103**, 153002 (2009).

[23] P. H. Bucksbaum, A. Zavriyev, H. G. Muller, and D. W. Schumacher, Softening of the H_2^+ molecular bond in intense laser fields, Phys. Rev. Lett. **64**, 1883 (1990).

[24] J. Ullrich, R. Moshammer, A. Dorn, R. Dörner, L. P. H. Schmidt, and H. Schmidt-Böcking, Recoil-ion and electron momentum spectroscopy: Reaction-microscopes, Rep. Prog. Phys. **66**, 1463 (2003).

[25] See Supplemental Material at http://link.aps.org/supplemental/10.1103/z4xn-m554 for detailed experimental methods, additional data, and theoretical derivations, which includes Refs. [2,5,17,23,24,26–43].

[26] X.-Y. Lai, C. Poli, H. Schomerus, and C. F. d. M. Faria, Influence of the Coulomb potential on above-threshold ionization: A quantum-orbit analysis beyond the strong-field approximation, Phys. Rev. A **92**, 043407 (2015).

[27] C. F. de M. Faria and A. S. Maxwell, It is all about phases: Ultrafast holographic photoelectron imaging, Rep. Prog. Phys. **83**, 034401 (2020).

[28] X. Lai, R. Sun, S. Yu, Y. Wang, W. Quan, A. Staudte, and X. Liu, Reconstructing molecular orbitals with laser-induced electron tunneling spectroscopy, Ultrafast Sci. **4**, 0038 (2024).

[29] A. Maxwell, A. Al-Jawahiry, T. Das, and C. F. d. M. Faria, Coulomb-corrected quantum interference in above-threshold ionization: Working towards multitrajectory electron holography, Phys. Rev. A **96**, 023420 (2017).

[30] T. Khurelbaatar, J. Heo, S. Yu, X. Lai, X. Liu, and D. E. Kim, Strong-field photoelectron holography in the subcycle limit, Light **13**, 108 (2024).

[31] C. T. L. Smeenk, L. Arissian, A. V. Sokolov, M. Spanner, K. F. Lee, A. Staudte, D. M. Villeneuve, and P. B. Corkum, Alignment dependent enhancement of the photoelectron cutoff for multiphoton ionization of molecules, Phys. Rev. Lett. **112**, 253001 (2014).

[32] R. Moshammer, M. Unverzagt, W. Schmitt, J. Ullrich, and H. Schmidt-Böcking, A 4π recoil-ion electron momentum analyzer: A high-resolution microscope for the investigation of the dynamics of atomic, molecular and nuclear reactions, Nucl. Instrum. Methods Phys. Res., Sect. B **108**, 425 (1996).

[33] R. Dörner, V. Mergel, O. Jagutzki, L. Spielberger, J. Ullrich, R. Moshammer, and H. Schmidt-Böcking, Cold target recoil ion momentum spectroscopy: A 'momentum microscope' to view atomic collision dynamics, Phys. Rep. **330**, 95 (2000).

[34] T. Jahnke, T. Weber, T. Osipov, A. Landers, O. Jagutzki, L. P. H. Schmidt, C. Cocke, M. Prior, H. Schmidt-Böcking, and R. Dörner, Multicoincidence studies of photo and auger electrons from fixed-in-space molecules using the COLTRIMS technique, J. Electron Spectrosc. Relat. Phenom. **141**, 229 (2004).

[35] M. J. Frisch, G. W. Trucks, H. B. Schlegel, G. E. Scuseria, M. A. Robb, J. R. Cheeseman, G. Scalmani, V. Barone, B. Mennucci, G. A. Petersson *et al.*, Gaussian 09, revision d.01 (Gaussian, Inc., Wallingford, CT, 2013).

[36] T. M. Yan, S. V. Popruzhenko, M. J. J. Vrakking, and D. Bauer, Low-energy structures in strong field ionization revealed by quantum orbits, Phys. Rev. Lett. **105**, 253002 (2010).

[37] A. S. Maxwell and C. F. de M. Faria, Quantum-orbit analysis of the effect of the Coulomb potential on the dynamics of atomic ionization by strong linearly polarized laser pulses, J. Phys. B **51**, 124001 (2018).

[38] E. Hasović, M. Busuladžić, W. Becker, and D. B. Milošević, Dressed-bound-state molecular strong-field approximation: Application to above-threshold ionization of heteronuclear diatomic molecules, Phys. Rev. A **84**, 063418 (2011).

[39] M. Kübel, M. Spanner, Z. Dube, A. Y. Naumov, S. Chelkowski, A. Bandrauk, M. Vrakking, P. Corkum, D. Villeneuve, and A. Staudte, Probing multiphoton light-induced molecular potentials, Nat. Commun. **11**, 2596 (2020).

[40] A. Rudenko, K. Zrost, T. Ergler, A. B. Voitkiv, B. Najjari, V. L. B. de Jesus, B. Feuerstein, C. D. Schröter, R. Moshammer, and J. Ullrich, Coulomb singularity in the transverse momentum distribution for strong-field single ionization, J. Phys. B **38**, L191 (2005).

[41] D. Comtois, D. Zeidler, H. Pépin, J. C. Kieffer, D. M. Villeneuve, and P. B. Corkum, Observation of Coulomb focusing in tunnelling ionization of noble gases, J. Phys. B **38**, 1923 (2005).

[42] J. Chen and C. H. Nam, Ion momentum distributions for he single and double ionization in strong laser fields, Phys. Rev. A **66**, 053415 (2002).

[43] R. Moshammer, J. Ullrich, B. Feuerstein, D. Fischer, A. Dorn, Crespo D. Schröter, J. R. C. Lopez-Urrutia, C. Hoehr, H. Rottke, C. Trump, M. Wittmann, G. Korn, and W. Sandner, Rescattering of ultralow-energy electrons for single ionization of Ne in the tunneling regime, Phys. Rev. Lett. **91**, 113002 (2003).

[44] W. Quan, Z. Lin, M. Wu, H. Kang, H. Liu, X. Liu, J. Chen, J. Liu, X. T. He, S. G. Chen, H. Xiong, L. Guo, H. Xu, Y. Fu, Y. Cheng, and Z. Z. Xu, Classical aspects in above-threshold ionization with a midinfrared strong laser field, Phys. Rev. Lett. **103**, 093001 (2009).

[45] T. Wang, Z. Dube, Y. Mi, G. Vampa, D. M. Villeneuve, P. B. Corkum, X. Liu, and A. Staudte, Disentangling interferences in the photoelectron momentum distribution from strong-field ionization, Phys. Rev. A **106**, 013106 (2022).